Ab initio study on crystal structure and phase stability of ZrC_2 under high pressure

Yong-Liang Guo(郭永亮), Jun-Hong Wei(韦俊红), Xiao Liu(刘潇), Xue-Zhi Ke(柯学志), and Zhao-Yong Jiao(焦照勇)

Citation: Chin. Phys. B, 2021, 30 (**1**): 016101. DOI: 10.1088/1674-1056/abb3e7
Journal homepage: http://cpb.iphy.ac.cn; http://iopscience.iop.org/cpb

What follows is a list of articles you may be interested in

Geoscience material structures prediction via CALYPSO methodology

Andreas Hermann
Chin. Phys. B, 2019, 28 (**10**): 106107. DOI: 10.1088/1674-1056/ab43bc

The CALYPSO methodology for structure prediction

Qunchao Tong(童群超), Jian Lv(吕健), Pengyue Gao(高朋越), Yanchao Wang(王彦超)
Chin. Phys. B, 2019, 28 (**10**): 106105. DOI: 10.1088/1674-1056/ab4174

Crystal structure and magnetic properties of disordered alloy $ErGa_{3-x}Mn_x$

Cong Wang(王聪), Yong-Quan Guo(郭永权), Shuo-Wang Yang(杨硕望)
Chin. Phys. B, 2019, 28 (**8**): 086101. DOI: 10.1088/1674-1056/28/8/086101

Isostructural phase transition-induced bulk modulus multiplication in dopant-stabilized ZrO_2 solid solution

Min Wang(王敏), Wen-Shu Shen(沈文舒), Xiao-Dong Li(李晓东), Yan-Chun Li(李延春), Guo-Zhao Zhang(张国召), Cai-Long Liu(刘才龙), Lin Zhao(赵琳), Shu-Peng Lv(吕舒鹏), Chun-Xiao Gao(高春晓), Yong-Hao Han(韩永昊)
Chin. Phys. B, 2019, 28 (**7**): 076109. DOI: 10.1088/1674-1056/28/7/076109

Crystal structures and decomposing of B-P compounds under pressure

Die Zhang(张蝶), Xilian Jin(靳锡联), Quan Zhuang(庄全), Ying Li(李颖), Shuhan Yang(杨淑涵), Liying Song(宋丽莹), Bingbing Liu(刘冰冰), Tian Cui(崔田)
Chin. Phys. B, 2019, 28 (**5**): 056101. DOI: 10.1088/1674-1056/28/5/056101

Ab initio study on crystal structure and phase stability of ZrC_2 under high pressure*

Yong-Liang Guo(郭永亮)[1,2,†], Jun-Hong Wei(韦俊红)[1], Xiao Liu(刘潇)[1], Xue-Zhi Ke(柯学志)[3], and Zhao-Yong Jiao(焦照勇)[2,‡]

[1] *School of Science and Henan Key Laboratory of Wire and Cable Structures and Materials, Henan Institute of Technology, Xinxiang* 453003, *China*
[2] *School of Physics, Henan Normal University, Xinxiang* 453007, *China*
[3] *School of Physics and Electronic Science, East China Normal University, Shanghai* 200241, *China*

(Received 4 May 2020; revised manuscript received 21 August 2020; accepted manuscript online 1 September 2020)

The structural stabilities and crystal evolution behaviors of the hyper stoichiometric compound ZrC_2 (carbon rich; C/Zr $>$ 1.0) are studied under ambient and high pressure conditions using first-principles calculations in combination with the particle-swarm optimization algorithm. Six viable structures of ZrC_2 in $P2_1/c$, $Cmmm$, $Cmc2_1$, $P4_2/nmc$, $Immm$ and $P6/mmm$ symmetries are identified. These structures are dynamically stable as their phonon spectra have no imaginary modes at zero pressure or at the selected high-pressure points. Among them, the $P2_1/c$ phase represents the ground state structure, whereas $P2_1/c$, $P4_2/nmc$, $Immm$ and $P6/mmm$ phases are part of the phase transition series. The phase order and critical pressures of the phase transition are determined to be approximately 300 GPa according to the equation of states and enthalpy. Furthermore, the mechanical and electronic properties are investigated. The $P2_1/c$ and $Cmc2_1$ phases display a semi-metal nature, whereas the $P4_2/nmc$, $Immm$, $P6/mmm$ and $Cmmm$ phases exhibit a metallic nature. Moreover, the present study reveals considerable information regarding the structural, mechanical and electronic properties of ZrC_2, thereby providing key insights into its material properties and evaluating its behavior in practical applications.

Keywords: crystal structure, phase transition, mechanical property, electronic band, first-principles calculation

PACS: 61.05.–a, 61.50.Ks, 62.20.–x, 62.50.–p **DOI:** 10.1088/1674-1056/abb3e7

1. Introduction

Transition metal carbides (TMCs), which comprise an interesting mixture of ionic, covalent and metallic bonding, have attracted considerable attention. These materials have been utilized in machining tools, the hard-coating industry, and aerospace applications owing to their extreme hardness, good thermal shock resistance, good chemical stability, high temperature mechanical strength, and high melting temperature.[1–4] As a TMC, zirconium carbide (ZrC) demonstrates potential for the application as a coating material for tri-isotropic (TRISO) nuclear fuel owing to its corrosion resistance against fission products, good thermal stability, better fission product retention capability, and neutron irradiation resistance.[5–9] Therefore, it can be used as an alternative to or supplemented with the currently used silicon carbide (SiC).[5,6]

Generally, ZrC exhibits cubic symmetry in the form of the B1 structure (space group: $Fm\bar{3}m$). Additionally, the Zr–C system appears to exhibit some amount, and often a large amount, of non-stoichiometry,[10] because the stoichiometric ZrC is represented in a narrow range, where even slight variations in processing parameters, such as temperature, reactant mass flow, or fluidizing gas flow rate, could result in either hypo- or hyper-stoichiometric compositions.[11] With the development of advanced computational methodologies, many non-stoichiometric compounds have been identified and provided new insights into the phase equilibria of this system. Recently, several studies[12–15] have investigated the stability of the hypo-stoichiometric Zr–C system (carbon deficient; C/Zr $<$ 1.0) using order-parameter functional (OPF), cluster expansion (CE) and evolutionary algorithm (EA) methods. Although their conclusions are varying in degree, it is found that Zr_7C_6 ($R\bar{3}$), Zr_4C_3 ($C2/c$), Zr_3C_2 ($Fddd$) and Zr_2C ($Fd\bar{3}m$) are stable hypo-stoichiometric phases of zirconium carbides. Moreover, the Zr–C system forms hyper-stoichiometric compounds (carbon rich; C/Zr $>$ 1.0).[8] Storms *et al.*[11] have reported that the material has both ZrC and C phases in the hyper-stoichiometric range. Vasudevamurthy *et al.*[8] have fabricated the carbon-rich sample, which has a hyper-stoichiometric composition of C/Zr $\sim$ 1.4. Are there any perfect hyper-stoichiometric Zr–C compounds such as Zr_2C_3 and ZrC_2? It is crucial to understand the microstructure of these materials, which is expected to have significant effects on the material properties. However, the research on these components is scarce.

Understanding the structural information and stability of

*Project supported by the National Natural Science Foundation of China (Grant Nos. 11904081 and 11975100), the Basic Research Program of Education Bureau of Henan Province, China (Grant No. 20A140007), and Research Initiation Fund of Henan Institute of Technology (Grant No. KQ1817).

†Corresponding author. E-mail: ylguo@hait.edu.cn
‡Corresponding author. E-mail: zhy_jiao@htu.cn

various stoichiometric components of the Zr–C system is essential for the safe operation of a TRISO fuel in a nuclear reactor. In this study, we focus on the hyper-stoichiometric compound ZrC_2, which is less studied. First, the crystal structures of ZrC_2 under ambient and high-pressure conditions are determined by performing an extensive structure search using first-principles calculations in combination with the particle-swarm optimization (PSO) algorithm.[16] Then, the thermodynamical and dynamical stabilities are investigated. The phase order and critical pressures with the pressure increasing are determined. Finally, the mechanical and electronic properties are studied comprehensively.

2. Theoretical methods

In this study, all calculations were performed within the density-functional-theory (DFT) framework with the projector augmented wave (PAW) scheme[17,18] using the Vienna *ab initio* simulation package (VASP).[19,20] To solve the Kohn–Sham equations, the exchange-correlation functional with the generalized gradient approximation (GGA) of the Perdew–Burke–Ernzerhof (PBE) scheme[21] was adopted. The kinetic energy cutoff was set to 800 eV. The structural predications of the global free energy minimization of ZrC_2 were performed using the CALYPSO code[22] based on the PSO methodology,[16] which has been proved to be effective in predicting the structure of various materials.[23–29] The ionic position, volume and shape of the structure cell were allowed to vary in their structural relaxations. The Brillouin-zone (BZ) of $P2_1/c$, $P4_2/nmc$, $Immm$, $P6/mmm$, $Cmc2_1$ and $Cmmm$ was sampled by k-point meshes of dimensions $6\times12\times6$, $8\times8\times12$, $12\times12\times12$, $16\times16\times16$, $20\times4\times8$ and $12\times12\times16$, respectively, generated via the Monkhorst–Pack scheme[30] for the primitive cell of ZrC_2. The forces on each ion convergence standard and the total energy convergence threshold were set to 0.001 eV/Å and 10^{-7} eV/atom, respectively.

The phonon dispersions were calculated using a supercell approach[31] as implemented in the PHONOPY code[32] to evaluate the dynamical stability of the crystal structures of various phases of ZrC_2. The principle of constructing supercells is based on the fact that the interaction force between two adjacent atoms moving with a small displacement in the cell is negligible. Therefore, the lattice constants a, b, and c in three directions of the constructed supercell were generally not less than 10 Å for each phase of ZrC_2. The BZ integration was performed using a $2\times2\times2$ k-point mesh. The symmetry nonequivalent zirconium atoms and carbon atoms were displaced from their equilibrium positions by the amplitude of 0.02 Å to construct the system dynamical matrix $D(k)$. The forces induced by the small displacements were calculated within the VASP code.

3. Results and discussions

3.1. Thermodynamically stable phases and structural properties

To obtain the possible phases of ZrC_2 under ambient and high pressure conditions, we determined its lower enthalpy structures based on the PSO methodology[16] in combination with the VASP package[19,20] with system sizes ranging from 1 to 8 chemical formula units (f.u.) per simulation cell at 0, 50, 100, 150 and 200 GPa. Further analysis of the enthalpy and stability leads to six possible stable or metastable structures up to 300 GPa, as illustrated in Fig. 1, namely, the $P2_1/c$, $Cmmm$, $Cmc2_1$, $P4_2/nmc$, $Immm$ and $P6/mmm$ phases. The calculated total energy per chemical f.u. versus the volume relations of the selected phases and the obtained results fitted by the third-order Birch–Murnaghan equation are plotted in Fig. 2. The enthalpies per chemical f.u. versus pressure are indicated in the inset of Fig. 2.

From Fig. 2, we can observe that the monoclinic $P2_1/c$ structure is the most stable phase below 5.8 GPa, indicating that this phase is the ground state of ZrC_2. The structure adopts the $P2_1/c$ symmetry and contains eight ZrC_2 f.u. per unit cell. One-dimensional armchair carbon chains along the a and b axes are observed in $P2_1/c$, as illustrated in Fig. 1(a). The tetragonal $P4_2/nmc$ structure is the most stable phase over the pressure range of 5.8–76.5 GPa, containing eight ZrC_2 f.u. per unit cell. In this phase, the carbon atoms form a saddle-shaped eight-membered ring, as illustrated in Figs. 1(d) and 1(d'). The other orthorhombic $Immm$ structure is the most stable phase over the pressure range of 76.5–253.6 GPa, containing four ZrC_2 f.u. per unit cell. One-dimensional carbon graphene-like ribbons are observed in $Immm$, as depicted in Figs. 1(e) and 1(e'). Above 253.6 GPa, $P6/mmm$ phase with an MgB_2-type structure is the most stable phase, containing one ZrC_2 f.u. per unit cell. The crystal structure of $P6/mmm$ is layered with alternative planes of pure zirconium atoms and pure carbon atoms. The carbon atoms form 2D graphene sheets, as depicted in Figs. 1(f) and 1(f'). According to the investigations of the total energy and enthalpy, the phase order and critical pressure of ZrC_2 due to the pressure increase can be expressed as $P2_1/c \xrightarrow{5.8\ \text{GPa}} P4_2/nmc \xrightarrow{76.5\ \text{GPa}} Immm \xrightarrow{253.6\ \text{GPa}} P6/mmm$. Interestingly, the enthalpies of the $Cmc2_1$, $Cmmm$, $P4_2/nmc$ and $Immm$ phases are significantly close to each other at approximately 75 GPa, although the $Cmc2_1$ and $Cmmm$ phases are not in the phase transition sequence, as depicted in the inset of Fig. 2. Additionally, the $Cmc2_1$ and $Cmmm$ phases are dynamically stable at 75 GPa according to the phonon dispersion curves (see Figs. 4(e) and 4(f)). This indicates that $Cmc2_1$ and $Cmmm$ are the metastable states of ZrC_2, and the $Cmc2_1$, $Cmmm$, $P4_2/nmc$ and $Immm$ phases may coexist and form a mixed phase at approximately 75 GPa.

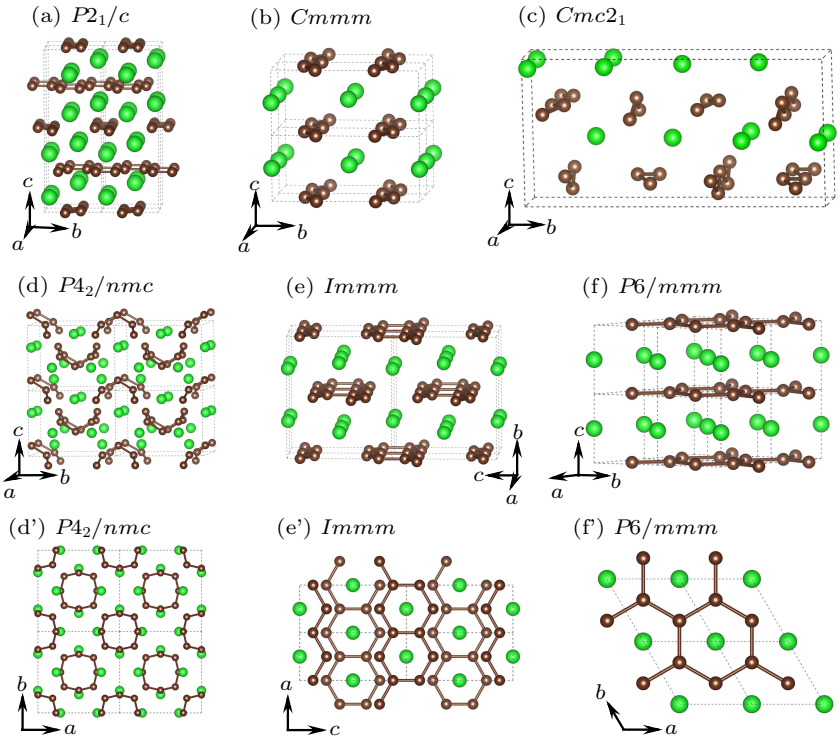

Fig. 1. Predicted crystal structures of ZrC_2 for (a) $P2_1/c$, (b) $Cmmm$, (c) $Cmc2_1$, (d), (d') $P4_2/nmc$, (e), (e') $Immm$ and (f), (f') $P6/mmm$ phases. The green and brown balls represent the zirconium and carbon atoms, respectively.

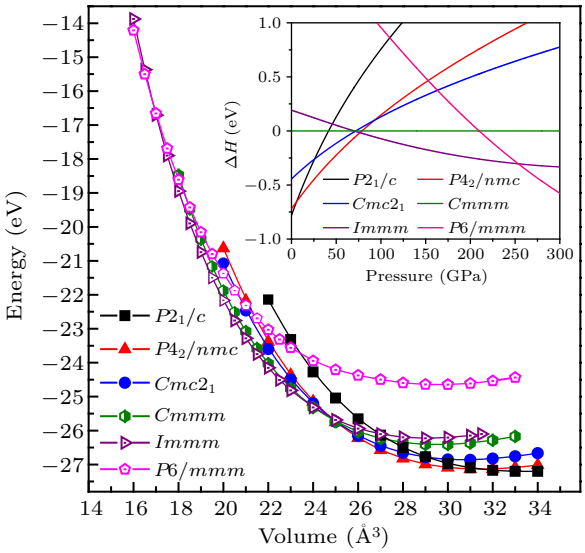

Fig. 2. Total energy versus volume results for the $P2_1/c$, $P4_2/nmc$, $Cmc2_1$, $Cmmm$, $Immm$ and $P4/mmm$ phases of ZrC_2. The inset depicts the calculated enthalpies versus pressure for the $P2_1/c$, $P4_2/nmc$, $Cmc2_1$, $Cmmm$, $Immm$ and $P4/mmm$ phases. The enthalpy of the $Cmmm$ phase is chosen as zero reference.

The formation energy was calculated to investigate the thermodynamic stability of ZrC_2. The *hcp*-Zr and graphite were used to calculate the energy of pure elements. The formation energies of Zr_xC_y were calculated by using the following equation:

$$\Delta H_{\text{formation}}(\text{Zr}_x\text{C}_y) = [H(\text{Zr}_x\text{C}_y) - xH(\text{Zr}) - yH(\text{C})]/(x+y). \quad (1)$$

The calculated formation energy of the $P2_1/c$ phase of ZrC_2 was -0.092 eV/atom. The negative formation energy of the $P2_1/c$ phase of ZrC_2 indicates that it is thermodynamically stable at ambient pressure and can be synthesized by experiment. Furthermore, we determined the formation energy of fcc ZrC, an experimentally synthesized material, to be -0.821 eV/atom. The formation energy of the $P2_1/c$ phase of ZrC_2 was higher than that of fcc ZrC, but lower than zero, indicating that the $P2_1/c$ phase is a metastable structure under ambient conditions. According to further enthalpy calculations, we obtained that the $P4_2/nmc$ phase of ZrC_2 is on the formation enthalpies covex hull for the stable phases of Zr–C system at 50 GPa, as shown in Fig. S1 in the Supporting Information, indicating that the ZrC_2 may be synthesized experimentally under high pressure.

Table 1. Calculated lattice parameters of $P2_1/c$, $P4_2/nmc$, $Immm$, $P6/mmm$, $Cmc2_1$ and $Cmmm$ phases of ZrC_2 under ambient conditions.

	Pressure	a_0 (Å)	b_0 (Å)	c_0 (Å)	α (°)	β (°)	γ (°)
$P2_1/c$	0 GPa	4.744	4.430	12.730	90.00	86.29	90.00
$P4_2/nmc$	0 GPa	6.965	6.965	5.180	90.00	90.00	90.00
$Immm$	0 GPa	2.703	7.106	6.046	90.00	90.00	90.00
$P6/mmm$	0 GPa	3.208	3.208	3.311	90.00	90.00	120.00
$Cmc2_1$	0 GPa	2.735	13.551	6.627	90.00	90.00	90.00
$Cmmm$	0 GPa	2.207	6.988	3.116	90.00	90.00	90.00

3.2. Dynamical stabilities

The phonon dispersion of a crystal is one of the fundamental subjects when considering the phase dynamical stability of a crystalline material. The dynamical instability of a crystal is associated with soft phonon modes that have imaginary frequencies.[33] To investigate the dynamical stabilities of the predicted phases, the phonon dispersion curves under ambient conditions were calculated and are depicted in Fig. 3. The phonon spectra reveal that the $P2_1/c$, $P4_2/nmc$ and $Cmc2_1$ phases of ZrC_2 exhibit no imaginary frequencies, indicating that these three phases are dynamically stable under ambient conditions. However, the longitudinal acoustic branch of the *Cmmm* phase exhibits a small imaginary frequency at the high-symmetry point Y (0.5, 0.5, 0.0) in BZ, as depicted in Fig. 3(d). The *Immm* phase exhibits some imaginary frequency, located between the high-symmetry points Γ (0, 0, 0) and X (0.5, −0.5, 0.5), as depicted in Fig. 3(e). The $P6/mmm$ phase exhibits significant imaginary frequency throughout BZ, as illustrated in Fig. 3(e), indicating that the phase is unstable under ambient conditions. Fortunately, further calculations reveal that the phonons of the *Cmmm*, *Immm* and $P6/mmm$ phases have no imaginary frequencies at the selected high-pressure points corresponding to the structural phase transitions, as depicted in Figs. 4(d)–4(f). These results indicate that the *Cmmm*, *Immm* and $P6/mmm$ phases are dynamically stable at the phase transition pressure. Additionally, the phonon dispersions of the phases $P2_1/c$ and $P4_2/nmc$, which are part of the phase transition sequence, exhibit no imaginary modes. The absence of phonon imaginary modes in the entire pressure range in this study demonstrates that the pressure-induced phase transitions of ZrC_2 are all driven by the energetics (i.e., the relative enthalpy change).

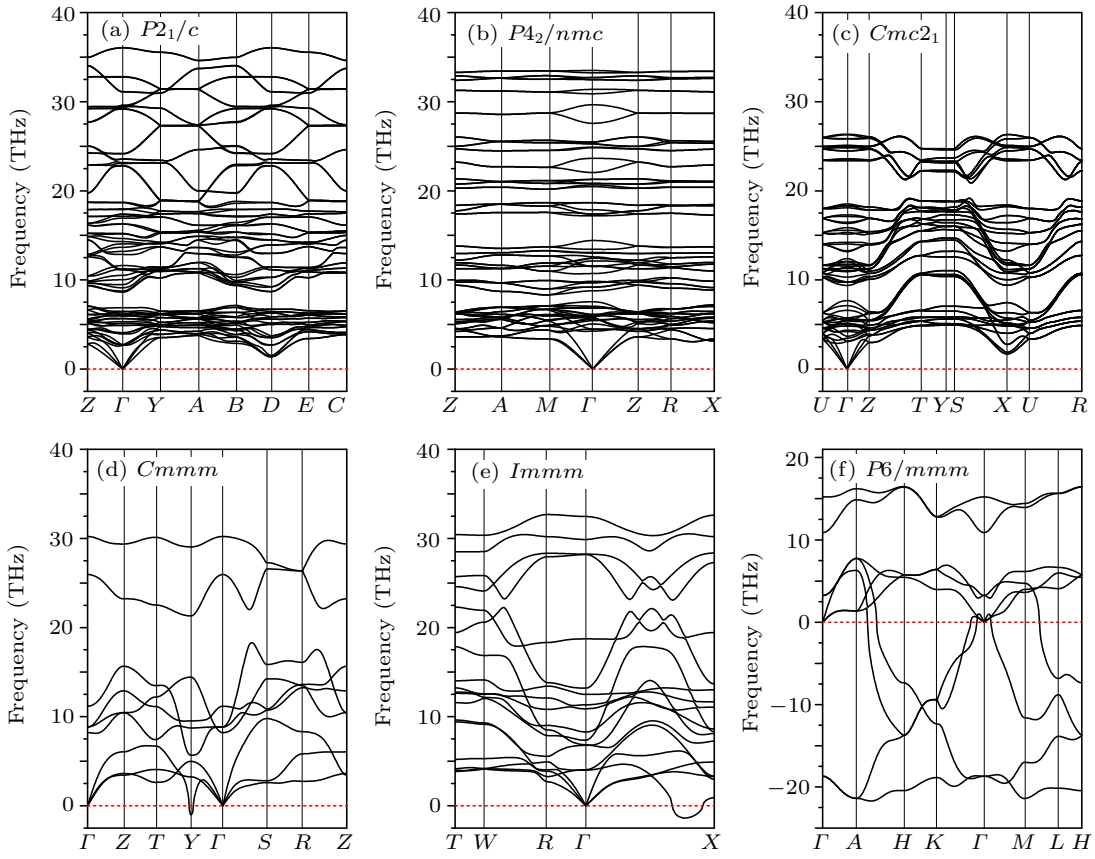

Fig. 3. Phonon dispersion curves for (a) $P2_1/c$, (b) $P4_2/nmc$, (c) $Cmc2_1$, (d) *Cmmm*, (e) *Immm* and (f) $P6/mmm$ phases of ZrC_2 under ambient conditions.

3.3. Mechanical properties

Elastic constants can provide information regarding the mechanical properties and stabilities of solids. To investigate the mechanical stabilities of the phases, we derived the second-order elastic constants (C_{ij}) from the strain-stress relationship[34] for the phases of ZrC_2, as listed in Table 2. The mechanical stability of any crystal requires the strain energy to be positive, implying that the entire set of elastic constants C_{ij} must satisfy the Born–Huang stability criteria.[35,36] In this work, the $P2_1/c$ is a monoclinic phase, in which the independent elastic stiffness tensor reduces to 13 components, namely, C_{11}, C_{22}, C_{33}, C_{44}, C_{55}, C_{66}, C_{12}, C_{13}, C_{23}, C_{15}, C_{25}, C_{35} and C_{46}. The corresponding mechanical stability criteria are given by $C_{11} > 0$, $C_{22} > 0$, $C_{33} > 0$, $C_{44} > 0$, $C_{55} > 0$, $C_{66} > 0$, $[C_{11}+C_{22}+C_{33}+2(C_{12}+C_{13}+C_{23})] > 0$, $(C_{33}C_{55} - C_{35}^2) > 0$, $(C_{44}C_{66} - C_{46}^2) > 0$, $(C_{22}+C_{33}-2C_{23}) > 0$, $[C_{22}(C_{33}C_{55} - C_{35}^2) + 2C_{23}C_{25}C_{35} -$

$C_{23}^2C_{55} - C_{25}^2C_{33}] > 0$, $\{2[C_{15}C_{25}(C_{33}C_{12} - C_{13}C_{23}) + C_{15}C_{35}(C_{22}C_{13} - C_{12}C_{23}) + C_{25}C_{35}(C_{11}C_{23} - C_{12}C_{13})] - [C_{15}^2(C_{22}C_{33} - C_{23}^2) + C_{25}^2(C_{11}C_{33} - C_{13}^2) + C_{35}^2(C_{11}C_{22} - C_{12}^2)] + C_{55}g\} > 0$. Here, $g = C_{11}C_{22}C_{33} - C_{11}C_{23}^2 - C_{22}C_{13}^2 - C_{33}C_{12}^2 + 2C_{12}C_{13}C_{23}$.[37,38] The $P4_2/nmc$ is a tetragonal phase, in which the independent elastic stiffness tensor reduces to six components of C_{11}, C_{33}, C_{44}, C_{66}, C_{12} and C_{13}. The corresponding mechanical stability criteria are given by $C_{11} > 0$, $C_{33} > 0$, $C_{44} > 0$, $C_{66} > 0$, $(C_{11} - C_{12}) > 0$, $(C_{11} + C_{33} - 2C_{13}) > 0$, $[2(C_{11} + C_{12}) + C_{33} + 4C_{13}] > 0$.[37,38] The $Immm$, $Cmc2_1$ and $Cmmm$ are orthorhombic phases, in which the independent elastic stiffness tensor reduces to nine components: C_{11}, C_{22}, C_{33}, C_{44}, C_{55}, C_{66}, C_{12}, C_{13} and C_{23}. The corresponding mechanical stability criteria are obtained by $C_{11} > 0$, $C_{22} > 0$, $C_{33} > 0$, $C_{44} > 0$, $C_{55} > 0$, $C_{66} > 0$, $[C_{11} + C_{22} + C_{33} + 2(C_{12} + C_{13} + C_{23})] > 0$, $(C_{11} + C_{22} - 2C_{12}) > 0$, $(C_{11} + C_{33} - 2C_{13}) > 0$, $(C_{22} + C_{33} - 2C_{23}) > 0$.[37,38] The $P6/mmm$ is a hexagonal phase, in which the independent elastic stiffness tensor reduces to five components: C_{11}, C_{33}, C_{44}, C_{12}, and C_{13}. The corresponding mechanical stability criteria are given by $C_{44} > 0$, $C_{11} > |C_{12}|$, $(C_{11} + 2C_{12})C_{33} > 2C_{13}^2$.[37,38] The elastic constants C_{ij} for the phases of ZrC_2 satisfy their respective mechanical stability criteria at zero and selected pressures, thus confirming their mechanical stability.

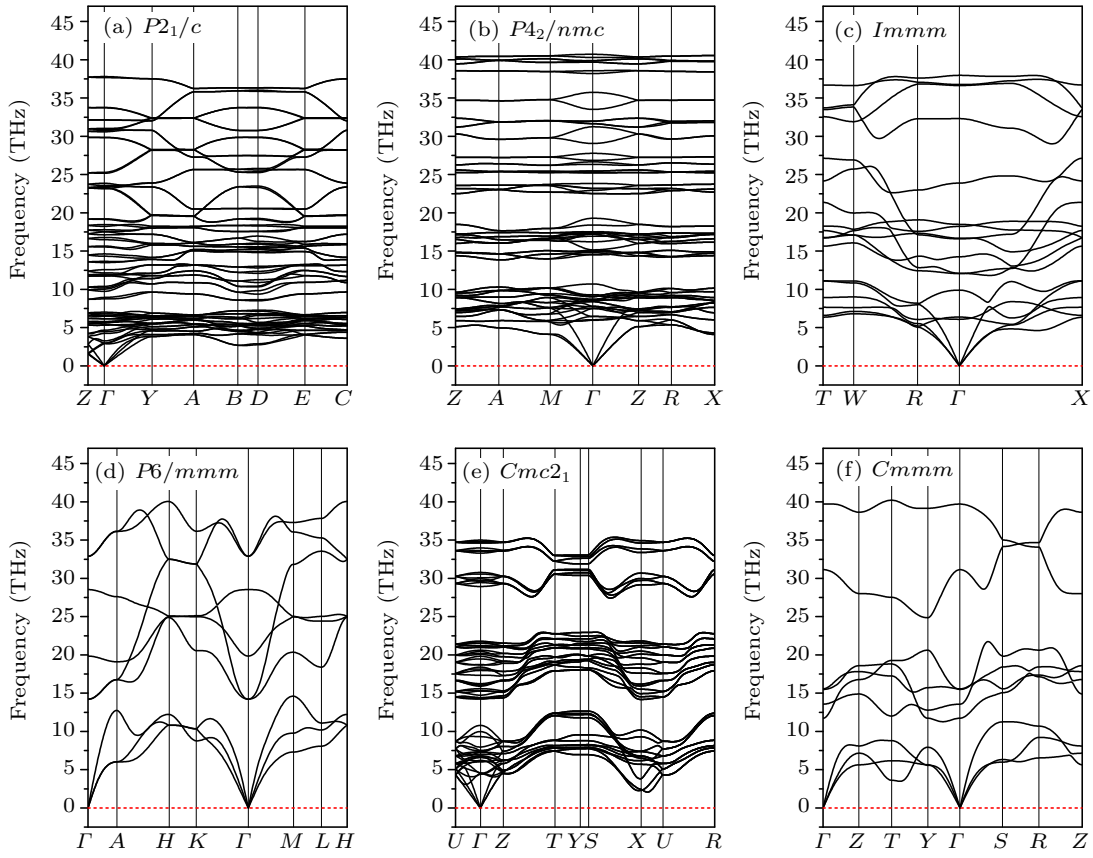

Fig. 4. Phonon dispersion curves for (a) $P2_1/c$, (b) $P4_2/nmc$, (c) $Immm$, (d) $P6/mmm$, (e) $Cmc2_1$ and (f) $Cmmm$ phases of ZrC_2 at 5.8, 76.5, 76.5, 253.6, 75 and 75 GPa, respectively.

Table 2. Calculated elastic constants C_{ij} for $P2_1/c$, $P4_2/nmc$, $Cmc2_1$, $Cmmm$, $Immm$ and $P6/mmm$ phases of ZrC_2 (in units of GPa).

	Pressure	C_{11}	C_{22}	C_{33}	C_{44}	C_{55}	C_{66}	C_{12}	C_{13}	C_{23}	C_{15}	C_{25}	C_{35}	C_{46}
$P2_1/c$	0 GPa	394.4	205.5	286.2	75.8	86.2	150.0	238.7	135.9	53.4	21.9	10.4	36.0	–2.3
$P4_2/nmc$	0 GPa	445.0		293.9	155.6		149.1	118.8	137.4					
$Immm$	76.5 GPa	792.3	1072.2	814.5	352.6	298.0	281.7	310.2	258.4	250.6				
$P6/mmm$	253.6 GPa	1116.3		1439.4	683.4		242.3	631.8	730.3					
$Cmc2_1$	75 GPa	1070.1	679.1	678.3	279.7	302.3	235.5	241.5	247.2	368.9				
$Cmmm$	75 GPa	663.5	1265.2	673.4	308.6	349.9	268.1	278.1	399.2	198.0				

Modulus is a fundamental parameter for characterizing the mechanical properties of materials. In terms of the Voigt–Reuss–Hill approximations,[39–41] the bulk modulus B, shear modulus G, Young's modulus E, Possion's ratio ν, Pugh's ratio (B/G) and log-Euclidean anisotropy index (A^{L}) of the phases of ZrC_2 are calculated based on the elastic constants, as listed in Table 3. For comparison, the previous reported elastic constants[42,43] of ZrC are listed in Table 3. From Ta-

ble 3, we can determine that the ZrC_2-P2_1/c phase is easier to be compressed than the ZrC-$Fm\bar{3}m$ phase under hydrostatic pressure, because the bulk modulus B of the former (153.8 GPa) is smaller than that of the latter (223 GPa[42]). The high pressure phase $P4_2/nmc$ of ZrC_2 exhibits approximately the same resistance to compression as the ZrC-$Fm\bar{3}m$ phase, as the bulk modulus B of the two phases are approximately the same. Other high pressure phases of ZrC_2 exhibit high B. However, we cannot indicate that these phases are difficult to be compressed because the data are calculated at nonequilibrium volume. Overall, the stiffness of ZrC_2 is lower than that of ZrC, because the B, G and E of the $P2_1/c$ and $P4_2/nmc$ phases for ZrC_2 are lower than those of ZrC-$Fm\bar{3}m$ at zero pressure.

Table 3. Calculated bulk modulus B (GPa), shear modulus G (GPa), Young's modulus E (GPa), Possion's ratio ν, Pugh's ratio (B/G) and log-Euclidean anisotropy index (A^{L}) for ZrC_2 and ZrC.

Material	Phase	Pressure	B	G	E	ν	B/G	A^{L}
ZrC_2	$P2_1/c$	0 GPa	153.8	73.2	189.5	0.295	2.101	1.348
	$P4_2/nmc$	0 GPa	215.8	141.9	349.2	0.231	1.521	0.095
	$Immm$	76.5 GPa	475.2	307.9	759.6	0.234	1.543	0.042
	$P6/mmm$	253.6 GPa	861.4	382.6	999.8	0.307	2.251	0.524
	$Cmc2_1$	75 GPa	456.7	257.0	649.2	0.263	1.777	0.195
	$Cmmm$	75 GPa	475.5	274.2	690.0	0.242	1.734	0.431
ZrC	$Fm\bar{3}m$	0 GPa	223[a]	170[a]	407[a]	0.18[b]	1.312[c]	0.012[d]

[a]Ref. [42]; [b]Ref. [43]; [c]computed with the values of elastic constants from Ref. [42]; [d]computed with the values of elastic constants from Ref. [43].

Poisson's ratio ν is a measure of a material tending to expand in directions perpendicular to the direction of compression, which usually ranges from -1 to 0.5. The larger the value of Poisson's ratio, the better the plasticity of the material. For example, most steels when utilized within their design limits (before yield) exhibit values of approximately 0.3, and rubber exhibits a Poisson's ratio of approximately 0.5. The ZrC-$Fm\bar{3}m$ exhibits a Poisson's ratio of 0.18,[43] demonstrating slight lateral expansion when compressed. The $P2_1/c$ and $P6/mmm$ phases of ZrC_2 exhibit approximately the same plasticity with steel, as their Poisson ratios are close to 0.3. Conversely, Poisson's ratio can further indicate the bonding type of a material, i.e., the value of ν for ionic and metallic materials is 0.25–0.33, and the covalent materials have smaller values of ν.[44] As presented in Table 3, the values of the phases of ZrC_2 are between 0.231 and 0.307, indicating that the compounds are expected to be ionic crystals.

Pugh's ratio (B/G) is often applied to evaluate the plastic behavior of a material, with 1.75 being the critical value.[45] A material will be ductile if $B/G > 1.75$, otherwise, it will be brittle.[46] As presented in Table 3, the calculated B/G's of $P2_1/c$ and $P6/mmm$ are 2.101 and 2.251, respectively, indicating that both of them are ductile in nature. Conversely, the $P4_2/nmc$ and $Immm$ are slightly brittle in nature as their B/G's are 1.521 and 1.543 (< 1.75), respectively. The other two phases of $Cmc2_1$ and $Cmmm$ are between ductile and brittle because their B/G's are approximately 1.75. However, the B/G of ZrC-$Fm\bar{3}m$ is 1.312, which is lower than that of all the phases of ZrC_2, suggesting that high content of carbon may lead to more ductile nature of Zr–C compounds.

The log-Euclidean anisotropic index A^{L} proposed by Christopher M. Kube provides an absolute measure of anisotropy in crystalline materials, which is valid for all the crystallite symmetries. Furthermore, it is generally used to describe the anisotropy of material.[47] It is calculated as

$$A^{\mathrm{L}} = \sqrt{\left[\ln\left(\frac{B^{\mathrm{V}}}{B^{\mathrm{R}}}\right)\right]^2 + 5\left[\ln\left(\frac{G^{\mathrm{V}}}{G^{\mathrm{R}}}\right)\right]^2}, \tag{2}$$

where B^{V} and B^{R} are the Voigt and Reuss bulk moduli, and G^{V} and G^{R} are the Voigt and Reuss shear moduli, respectively. If $A^{\mathrm{L}} = 0$, it refers to a locally isotropic single crystal, and a larger A^{L} implies a more pronounced anisotropic. From Table 3, we observe that the A^{L} of ZrC-$Fm\bar{3}m$ is 0.012, which is significantly close to zero, indicating that it is almost isotropic. For ZrC_2, the $P2_1/c$ phase exhibits the highest degree of anisotropy, as its A^{L} equals 1.348, which is far away from zero. The $P6/mmm$, $Cmc2_1$ and $Cmmm$ phases exhibit weaker anisotropy, and the $P4_2/nmc$ and $Immm$ phases exhibit an almost isotropic nature.

3.4. Electronic and bonding properties

To investigate the electronic properties of ZrC_2, we calculate the electronic band structures of the phases at the selected pressure, as depicted in Fig. 5. The Fermi level is set at zero. From the figure, we can observe that the ground state phase $P2_1/c$ and the metastable phase $Cmc2_1$ exhibit a semimetal nature because they have an indirect negative band gap. Specifically, the conduction band minima lie lower than the valence band maxima. For the $P2_1/c$ phase, the conduction band minima is approximately -0.144 eV, located between points B and D, and the valence band maxima is approximately 0.109 eV, located between points E and C, as depicted in Fig. 5(a). We further calculate the electronic band structure for $P2_1/c$ phase using HSE06 hybrid functional, and the

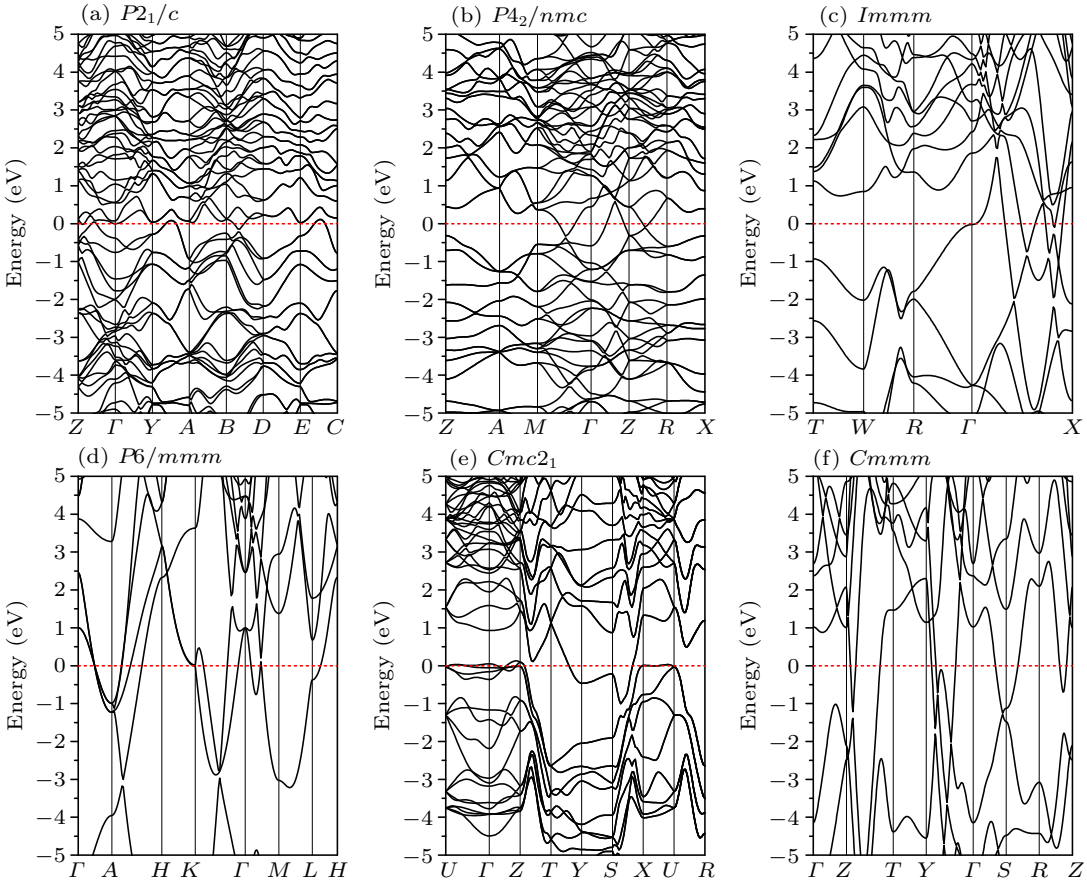

Fig. 5. Electronic band structures for (a) $P2_1/c$, (b) $P4_2/nmc$, (c) $Immm$, (d) $P6/mmm$, (e) $Cmc2_1$ and (f) $Cmmm$ phases of ZrC_2 at 0, 0, 76.5, 253.6, 75 and 75 GPa, respectively.

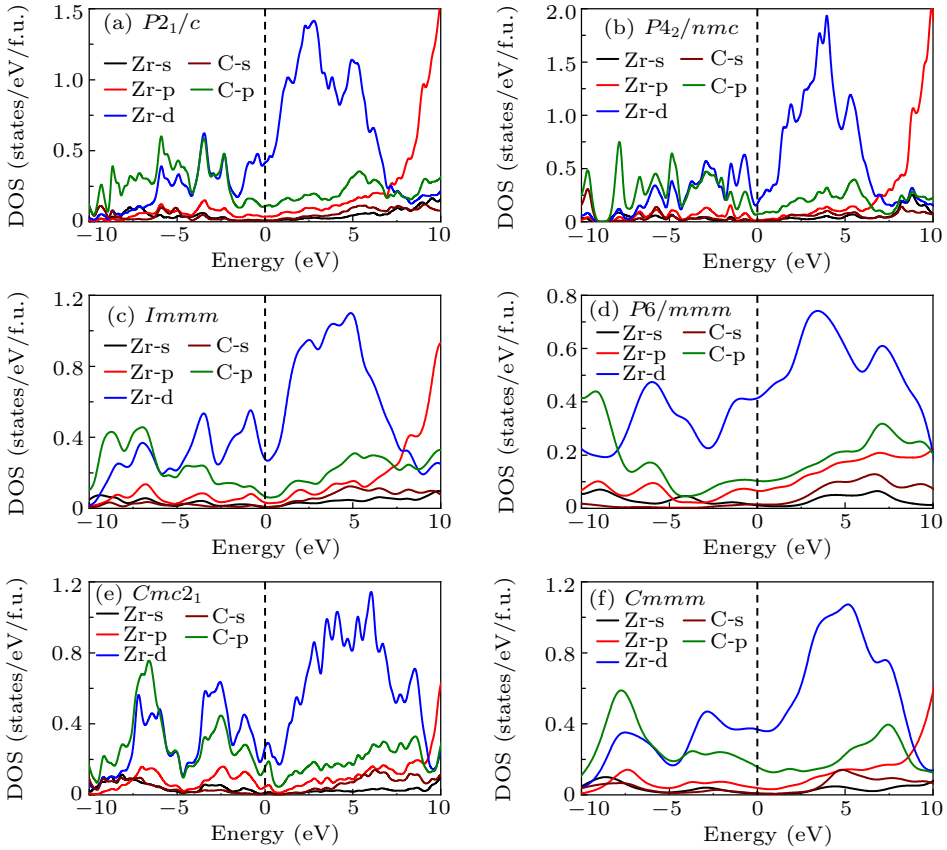

Fig. 6. Electronic density of states (DOS) for (a) $P2_1/c$, (b) $P4_2/nmc$, (c) $Immm$, (d) $P6/mmm$, (e) $Cmc2_1$ and (f) $Cmmm$ phases of ZrC_2 under 0, 0, 76.5, 253.6, 75 and 75 GPa, respectively.

negative band gap for this phase at PBE level does not change to a positive band gap at HSE level, as shown in Fig. S2 in the Supporting Information. The semi-metallic nature of the $P2_1/c$ phase is unlikely to be affected since the steep band crossing near the Fermi energy is insensitive to the choice of the functional used, and calculations using more accurate hybrid functionals do not open a band gap in this system. Therefore, we infer that the PBE functional can be expected to return accurate results for the electronic band structure calculations of semi-metal materials. For the $Cmc2_1$ phase, the conduction band minima is approximately -1.002 eV, located between points S and X, and the valence band maxima is approximately 0.127 eV, located between points Γ and Z, as illustrated in Fig. 5(e). The $P4_2/nmc$, $Immm$, $P6/mmm$ and $Cmmm$ phases exhibit metallic nature with the band crossing Fermi level. For the further investigation of the elemental contributions to the electronic structure of these phases, the projected density of states (PDOS) were calculated as depicted in Fig. 6. From the figures of DOS, we can observe that all the phases exhibit semi-metal or metallic nature because of their finite DOS at the Fermi level. The PDOSs are observed to be similar and suggest that the bands close to the Fermi level are mainly the Zr-d states of all the phases.

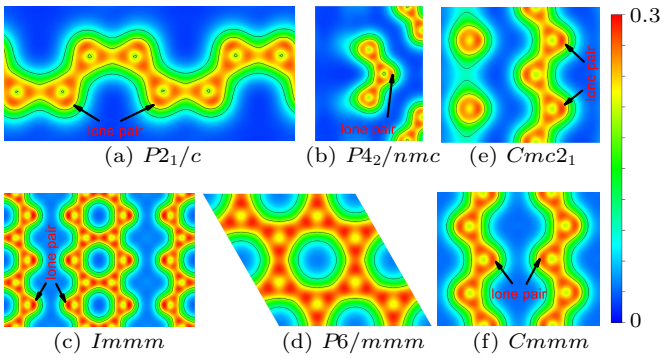

Fig. 7. Charge density distribution of the selected plane for (a) $P2_1/c$, (b) $P4_2/nmc$, (c) $Immm$, (d) $P6/mmm$, (e) $Cmc2_1$ and (f) $Cmmm$ phases of ZrC_2 under 0, 0, 76.5, 253.6, 75 and 75 GPa, respectively. The selected planes are shown in Fig. S3 of the Supporting Information. The contour interval is 0.1 electrons/Bohr^3.

To explore the bonding character of ZrC_2, we calculate the charge density distribution of the phases at the selected pressure, as shown in Fig. 7. It is well known that the near spherical distribution of electron density indicates an ionic character, and the electron density along the bond indicates a covalent character.[48] Our results demonstrate that the various phases of ZrC_2 have the similar charge density distribution, that is to say, the charge density is centered around Zr atoms and there is a small amount of charge density between Zr and C atoms, while a large amount of density is distributed along the C–C bond. It is indicated that the bond between the Zr and C has more ionic character, while the C–C bond has covalent character. Interestingly, the charge density distribution demonstrates that all of the phases have a stable and localized lone-pair (non-bonding state) at the external corner of the carbon chains or ribbons except the $P6/mmm$ phase.

4. Conclusion

In this work, we have conducted a systematic study of the hyper stoichiometric compound ZrC_2 using first-principles calculations in combination with the particle-swarm optimization algorithm. We have determined the stable structures, phase stabilities, phase order and critical pressures due to the pressure increase for the fundamental understanding and practical applications of the Zr–C compounds in the TRISO fuel system. Six possible stable or metastable structures are identified, namely, $P2_1/c$, $Cmmm$, $Cmc2_1$, $P4_2/nmc$, $Immm$ and $P6/mmm$ phases. According to the calculated total energy and enthalpy of these phases, we find that the $P2_1/c$ phase is the ground state structure of ZrC_2, whereas the phase order and critical pressures are $P2_1/c \xrightarrow{5.8\ \text{GPa}} P4_2/nmc \xrightarrow{76.5\ \text{GPa}} Immm \xrightarrow{253.6\ \text{GPa}} P6/mmm$ with pressure increasing. Although the $Cmc2_1$ and $Cmmm$ phases are not contained in the phase transition sequence, their enthalpies are significantly close to those of the $P4_2/nmc$ and $Immm$ phases at approximately 75 GPa. This demonstrates that the four phases $Cmc2_1$, $Cmmm$, $P4_2/nmc$ and $Immm$ may coexist and form a mixed phase at approximately 75 GPa.

The phonon dispersion curves of $P2_1/c$, $P4_2/nmc$ and $Cmc2_1$ exhibit no imaginary modes in the entire BZ at zero pressure, and all the predicted phases exhibit no imaginary frequencies at the selected high-pressure points. These results indicate that all the predicted phases of ZrC_2 are dynamically stable at zero pressure or at the phase transition pressure. The calculated elastic constants C_{ij} reveal that the phases of ZrC_2 are mechanically stable at zero or at selected pressures because their C_{ij} satisfy the Born–Huang mechanical stability criteria. Furthermore, the bulk modulus B, shear modulus G, Young's modulus E, Possion's ratio ν, Pugh's ratio (B/G) and log-Euclidean anisotropy index (A^{L}) are investigated based on the Voigt–Reuss–Hill approximations. The results indicate that the ground state ZrC_2 $P2_1/c$ phase is easier to be compressed than the ZrC-$Fm\bar{3}m$ phase under hydrostatic pressure. However, the high pressure phase $P4_2/nmc$ of ZrC_2 demonstrates approximately the same resistance to compression as the ZrC-$Fm\bar{3}m$ phase. Comparing Pugh's ratios (B/G) of ZrC_2 and ZrC, we can realize that the high content of carbon may lead to the more ductile nature of the Zr–C compounds, because the B/G of ZrC-$Fm\bar{3}m$ is lower than those of all the phases of ZrC_2. The log-Euclidean anisotropic index A^{L} reveals that the $P2_1/c$ phase exhibits the highest degree of anisotropy; the $P6/mmm$, $Cmc2_1$ and $Cmmm$ phases exhibit weaker anisotropy; and the $P4_2/nmc$ and $Immm$ phases demonstrate almost isotropic nature. The calculated electronic band structures of ZrC_2 demonstrate that the ground state

phase $P2_1/c$ and the metastable phase $Cmc2_1$ exhibit semimetal nature and the phases $P4_2/nmc$, $Immm$, $P6/mmm$ and $Cmmm$ exhibit metallic nature.

In summary, the results reported here provide a comprehensive description of the structural stabilities, and mechanical and electronic properties of ZrC_2 over a wide range of pressure. This information is crucial for understanding the structural evolution under high pressure and evaluating the behavior of Zr–C compounds in the application of the clad material for the TRISO fuel. The theoretical predictions about the crystal structures, the phase transitions and the physical properties of ZrC_2 under ambient and high pressure conditions call for further experimental investigation and exploration.

Acknowledgment

This work was supported by the High Performance Computing Center of Henan Normal University.

References

[1] Levine S R, Opila E J, Halbig M C, Kiser J D, Singh M and Salem J A 2002 *J. Eur. Ceram. Soc.* **22** 2757
[2] Opeka M M, Talmy I G and Zaykoski J A 2004 *J. Mater. Sci.* **39** 5887
[3] Savino R, Fumo M D S, Paterna D and Serpico M 2005 *Aerospace Sci. Technol.* **9** 151
[4] Li H, Zhang L, Zeng Q, Guan K, Li K, Ren H, Liu S and Cheng L 2011 *Solid State Commun.* **151** 602
[5] Katoh Y, Vasudevamurthy G, Nozawa T and Snead L L 2013 *J. Nucl. Mater.* **441** 718
[6] Porter I E, Knight T W, Dulude M C, Roberts E and Hobbs J 2013 *Nucl. Engin. Design* **259** 180
[7] Snead L L, Katoh Y and Kondo S 2010 *J. Nucl. Mater.* **399** 200
[8] Vasudevamurthy G, Katoh Y, Aihara J, Sawa K and Snead L L 2015 *J. Nucl. Mater.* **464** 245
[9] Kim D, Chun Y B, Ko M J, Lee H G, Cho M S, Park J Y and Kim W J 2016 *J. Nucl. Mater.* **479** 93
[10] Weinberger C R and Thompson G B 2018 *J. Am. Ceram. Soc.* **101** 4401
[11] Storms E 1967 *The refractory carbides* (New York: Academic Press)
[12] Gusev A I and Rempel A A 1994 *J. Phys. Chem. Solids* **299** 14
[13] Zhang Y, Liu B and Wang J 2016 *Sci. Rep.* **5** 18098
[14] Yu X X, Weinberger C R and Thompson G B 2016 *Comput. Mater. Sci.* **112** 318
[15] Xie C, Oganov A R, Li D, Debela T T, Liu N, Dong D and Zeng Q 2016 *Phys. Chem. Chem. Phys.* **18** 12299
[16] Wang Y C, Lv J, Zhu L and Ma Y M 2010 *Phys. Rev. B* **82** 094116
[17] Blöchl P E 1994 *Phys. Rev. B* **50** 17953
[18] Kresse G and Joubert D 1999 *Phys. Rev. B* **59** 1758
[19] Kresse G and Furthmüller J 1996 *Phys. Rev. B* **54** 11169
[20] Kresse G and Furthmüller J 1996 *Comput. Mater. Sci.* **6** 15
[21] Perdew J P, Burke K and Ernzerhof M 1996 *Phys. Rev. Lett.* **77** 3865
[22] Wang Y C, Lv J, Zhu L and Ma Y M 2012 *Comput. Phys. Commun.* **183** 2063
[23] Lv J, Wang Y C, Zhu L and Ma Y M 2011 *Phys. Rev. Lett.* **106** 015503
[24] Li Q, Zhou D, Zheng W, Ma Y and Chen C 2013 *Phys. Rev. Lett.* **110** 136403
[25] Zhang M, Liu H, Li Q, Gao B, Wang Y, Li H, Chen C and Ma Y 2015 *Phys. Rev. Lett.* **114** 015502
[26] Zhang G T, Bai T T, Yan H Y and Zhao Y R 2015 *Chin. Phys. B* **24** 106104
[27] Guo Y L, Wang C Y, Qiu W J, Ke X Z, Huai P, Cheng C, Zhu Z Y and Chen C F 2016 *Phys. Rev. B* **94** 134104
[28] Peng F, Sun Y, Pickard C J, Needs R J, Wu Q and Ma Y 2017 *Phys. Rev. Lett.* **119** 107001
[29] Sun Y, Xu B and Yi L 2020 *Chin. Phys. B* **29** 023102
[30] Monkhorst H J and Pack J D 1976 *Phys. Rev. B* **13** 5188
[31] Parlinski K, Li Z Q and Kawazoe Y 1997 *Phys. Rev. Lett.* **78** 4063
[32] Togo A, Oba F and Tanaka I 2008 *Phys. Rev. B* **78** 134106
[33] Cochran W 1959 *Phys. Rev. Lett.* **3** 412
[34] Page Y L and Saxe P 2002 *Phys. Rev. B* **65** 104104
[35] Born M 1940 *Math. Proc. Cambridge Philos. Soc.* **36** 160
[36] Born M and Huang K 1954 *Dynamical theory of crystal lattices* (New York: Clarendon Press)
[37] Wu Z J, Zhao E J, Xiang H P, Hao X M, Liu X J and Meng J 2007 *Phys. Rev. B* **76** 054115
[38] Mouhat F and Coudert F X 2014 *Phys. Rev. B* **90** 224104
[39] Voigt W 2014 *Lehrbuch der Kristallphysik (MIT Ausschlußder Kristalloptik)* (Wiesbaden: Springer-Verlag)
[40] Reuss A 1929 *J. Appl. Math. Mech. Z. Angew. Math. Mech.* **9** 49
[41] Hill R 1952 *Proc. Phys. Soc. Sect. A* **65** 349
[42] Green D J 1988 *An introduction to the mechanical properties of ceramics* (Cambridge: Cambridge University Press)
[43] Fu H, Peng W and Gao T 2009 *Mater. Chem. Phys.* **115** 789
[44] Haines J, Leger J and Bocquillon G 2001 *Annu. Rev. Mater. Res.* 2001 **31** 1
[45] Pugh S F 1954 *Philo. Mag.* **45** 823
[46] Kutepov A L and Kutepova S G 2003 *Phys. Rev. B* **67** 132102
[47] Kube C M 2016 *AIP Adv.* **6** 095209
[48] Aydin S, Tatar A and Ciftci Y O 2012 *J. Nucl. Mater.* **429** 55